



# ANTARES: R&D Project for a Multipurpose Detector

C. Carloganu

► **To cite this version:**

C. Carloganu. ANTARES: R&D Project for a Multipurpose Detector. Topical Seminar On Neutrino And AstroParticle Physics 6, May 1999, San Miniato, Italy. pp.146-152. in2p3-00022435

**HAL Id: in2p3-00022435**

**<http://hal.in2p3.fr/in2p3-00022435>**

Submitted on 1 Dec 2000

**HAL** is a multi-disciplinary open access archive for the deposit and dissemination of scientific research documents, whether they are published or not. The documents may come from teaching and research institutions in France or abroad, or from public or private research centers.

L'archive ouverte pluridisciplinaire **HAL**, est destinée au dépôt et à la diffusion de documents scientifiques de niveau recherche, publiés ou non, émanant des établissements d'enseignement et de recherche français ou étrangers, des laboratoires publics ou privés.

## ANTARES – R&D project for a multipurpose detector

C. Cârloganu<sup>a</sup>

<sup>a</sup>Centre de Physique des Particules de Marseille, CNRS/IN2P3 — Univ Méditerranée,  
163 Avenue de Luminy, Case 907, 13288 Marseille Cedex 9, France

On behalf of the ANTARES collaboration

Over the last three years, the ANTARES collaboration had an intensive R&D activity for the construction of a deep-sea neutrino telescope. The site, the procedures and the performances of the proposed detector were evaluated. The deployment and the underwater electrical connections were tested successfully at 2400 m depth, in the Mediterranean Sea, near Toulon, in the proposed site for the first phase of the project. This phase consists in the deployment of a detector with an effective area of about 0.1 km<sup>2</sup> by 2002.

### 1. The ANTARES project

In 1996, a collaboration of particle physicists, astrophysicists and experts in marine technology was formed to build a deep sea neutrino telescope. A first phase of R&D finished in 1999, when the construction of a detector with an effective area of about 0.1 km<sup>2</sup> was approved.

The ANTARES scientific program [1] reflects the interdisciplinary nature of the collaboration. The main motivation comes from neutrino astronomy, since the detection of the cosmic neutrinos would lead to a better understanding of several astrophysical environments, from the supposed accelerators of the UHE cosmic rays, to high density regions, opaques to photons (astrophysical beam-dumps). The neutrinos would result from the charged pions produced by the interaction of accelerated protons with matter ( $pp$ ) or radiation ( $p\gamma$ ). Candidate sources of high energy neutrinos include X-ray binaries and supernova remnants, active galactic nuclei (AGN) and gamma-ray bursters (GRB).

Dark matter could be detected via high energy neutrinos if supersymmetric neutralinos account for (part of) the missing mass of the universe. Neutralinos would accumulate in the core of heavy bodies such as the earth, the sun or the center of the galaxy and their annihilation would lead to a constant flux of neutrinos, with an angular distribution depending on the neutralino mass.

For the study of the atmospheric neutrinos, ANTARES benefits from an oscillation baseline length of the order of the earth diameter. For the SuperKamiokande oscillation parameters ( $\Delta m^2 = 3.5 \cdot 10^{-3} \text{ eV}^2$ ,  $\sin^2 \theta = 1$ ) [2], the first dip in the survival probability of the neutrinos crossing the earth occurs at 350 km/GeV, at the maximum of the ANTARES sensitivity.

Long term observations of the deep sea environment will be also pursued, being of particular interest for biologists and sea scientists.

### 2. Proposed detector

In the first phase of the project, 13 strings carrying about 1000 photomultipliers (PMTs) in total will be deployed. The positions of the strings are randomized along a spiral, with a minimal spacing of about 60 m (Figure 1, detector top view).

On one string, the PMTs, housed in pressure resistant glass spheres are clusterized by three in a storey and oriented down-looking at 45° from the vertical. The design ensures a good efficiency for up-going tracks and only a marginal acceptance for the down going ones. In the same time, the overlap in the active solid angle for the PMTs in a cluster allows an event trigger based on local coincidences in a storey.

The spacing of the clusters along the string is of 8 m for the inner four strings, and 16 m for the outer nine. With 41 storeys in the dense strings and 21 on the sparse ones, the instru-

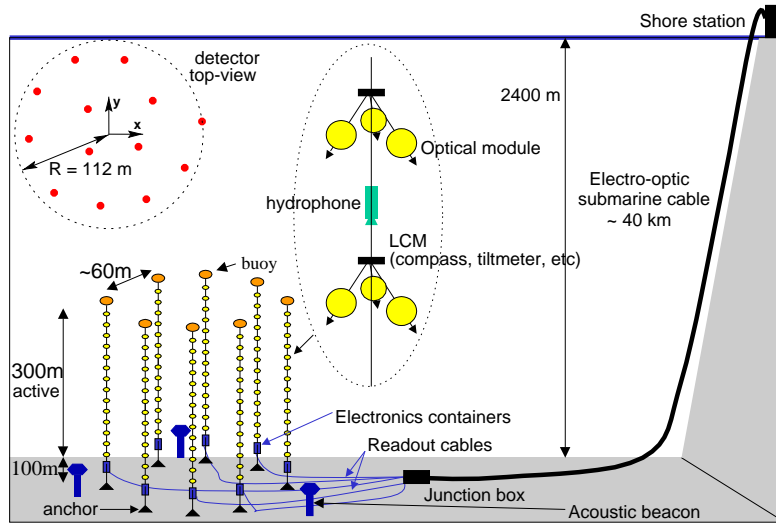


Figure 1. Schematic diagram of the first phase of the ANTARES detector.

mented height of the string is of 320 m. A 100 m of non-instrumented length is foreseen to the bottom of each string. The strings are flexible — the mechanical structure is ensured by an electro-mechanical cable.

On the same optical module frame, which supports the three optical modules, a special container houses a local control module (LCM), calibration equipment, a compass and a tiltmeter. In order to facilitate the data acquisition, about 6 LCM's are grouped together in a master LCM, which gathers all the information before sending it to the string control module (SCM), located at the bottom of the string. Electrical cables connect all the SCMs to a junction box, which is linked to the shore station by a standard deep sea telecommunications cable.

The off-shore trigger logic will be as simple as possible [1]. A first level trigger requires a coincidence of two of the three OMs serviced by a LCM. The second-level trigger will be based on a combination of first-level triggers. If a second-level trigger occurs, the full detector will be read out. The third level trigger will be made on shore.

The first-level rate is estimated to about 150 kHz, and the second level rate to a few kHz. The third level should not pass over 100 Hz, to be recorded for off-line analysis.

In each optical module, an electronic board digitizes the PMT signals before storing them in a pipeline memory, which is read if a second level trigger occurs. A pulse shape discriminator selects single photo-electron pulses (99% of the overall PMT pulses) from more complex signals. In the first case, only the charge and the time information are stored, whereas in the second the full waveform is digitized.

### 2.1. Positioning

Of special importance for a neutrino telescope is the positioning of the detector. For neutrino source pointing, an absolute orientation with respect to the sky of about  $0.2^\circ$  is necessary. It will be obtained by triangulation of acoustical beacons (one at the bottom of each string) with the surface boat, coupled with DGPS. Supplementary ones will be distributed around the detector in order to have a precise positioning of the outer strings.

The precision of the PMTs relative positioning influences directly the angular resolution on the muon tracks. A precision of 1.3 cm can be obtained by the triangulation of the hydrophones distributed along the string with the acoustical beacons from the neighbouring strings [1]. The PMTs orientation is reconstructed using the data from the associated tiltmeters and compasses.

## 2.2. Prototype testing

Complete prototype strings have been immersed to test the deployment technique, instrumentation and slow control. The strings will be deployed vertically and their recovery is activated by an acoustical signal from the surface which disconnects the string from its anchoring weight. The undersea electrical connection of the SCMs to the junction box has been successfully tested with a manned submarine in December 98.

A 350 m prototype string, with 8 optical modules, fully equipped with the positioning system will be deployed during the summer 99. It will be connected to the shore station 40 km away with an electro-optical cable. Slow control and experimental data will be sent to the shore.

## 3. Site characterization

The selection of a suitable site for a neutrino telescope requires consideration of water transparency, optical background, fouling of the optical surfaces, strength of the deep sea currents, meteorological conditions, depth, on-shore support and infrastructure. A site 20 nautical miles off the coast from Toulon, in the Mediterranean sea (42°50' N, 6°10' E), at a depth of 2400 m has been explored and chosen for the deployment of the 0.1 km<sup>2</sup> detector.

Weather conditions on the site have been studied using the available meteorological data, which include wind speed and direction, wave height. The analysis of 4 years of data allowed the identification of the periods with favorable sea conditions for the deployment.

The sea floor at the site, explored with a submarine, is flat. The analysis of the cores recovered from the bottom showed that they consist of solid mud, which is an adequate floor for the

deployment of the detector.

Salinity and temperature (13.2°) are extremely stable. The highest recorded value for the current speed is 17 cm/s (the average is less than 3 cm/s), but values as high as 30 cm/s were considered in the design of the detector lines, since it has an important impact on the mechanical lay-out and on the minimal spacing of the strings [1].

Fouling occurs on the modules, due to the sedimentation and to the growth of bacteria on the surfaces. A long term measurement (eight months of immersion) has been performed in order to study the loss of transmission on a vertical surface (PMT looking horizontally). The measured value of 1.5% is an upper limit on the fouling rate in the future detector, since in the detector design the optical module axes will be oriented at a polar angle of 135°.

The optical properties of the site have also important consequences on the detector design and performances. Different tests have been designed and repeated several times over the last three years in order to measure the light transmission and the deep sea optical background [3].

### 3.1. Water transparency

The transparency of the medium in which the photons propagate has important consequences both on the angular resolution for the muon track reconstruction and on the effective volume of the detector. The longer the scattering length of the photons, the less they will be deflected from their original direction and therefore the directional information about the muon track generating them will be preserved over longer distances.

In December 97, the attenuation length was measured with a 33 m long structure, holding a collimated, continuous LED source located at a variable distance from a glass sphere containing a 8" PMT. For a wavelength of 466 nm (this is roughly where our global transmission efficiency is expected to peak),

$$\lambda_{\text{att,eff}} = 41 \pm 1(\text{stat.}) \pm 1(\text{syst.}) \text{ m} \quad (1)$$

The attenuation length results from a combination of absorption and scattering. A second test was therefore designed to disentangle the two contributions.

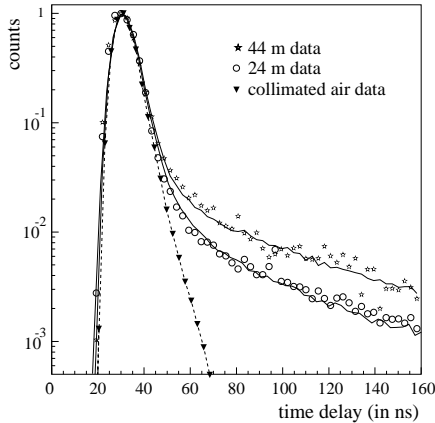


Figure 2. Distribution of photon arrival times for the collimated air spectrum (dashes) and for two spectra taken *in situ*, with source-deflector distances  $D$  of 24 m and 44 m. All spectra are normalized to a maximum of 1. *In situ* spectra are corrected for the  $1/D^2$  decrease. The Monte Carlo spectra for the best fit values are overlaid (solid curve) on the top of the data.

In July 98 and March 99, the arrival time of the photons from a pulsed isotropic LED source (466 nm) situated at a distance of either 24 m or 44 m away from a 1" fast PMT was measured. The distribution (Figure 2) displays a clear peak coming from the direct photons, exceeding by several orders of magnitude the tail due to the scattered photons. At 24 m (44 m), the ratio of scattered to direct photons is less than 5% (10%).

An effective attenuation length was inferred from the ratio of the integrated spectra measured at the two distances, yielding:

$$\lambda_{\text{att. eff}} = \begin{cases} 60.0 \pm 0.4(\text{stat.}) \text{ m (July 98)} \\ 52.2 \pm 0.7(\text{stat.}) \text{ m (March 99)} \end{cases} \quad (2)$$

A systematic uncertainty of a few meters, coming from the LED luminosity calibration might affect these estimates. The difference between the first measurement and those obtained with the pulsed source are partially accounted for by the collimation of the source in the first case, whereas an isotropic source was used in the second. The

source (an)isotropy changes the “effective attenuation length” by about 10%. The different measurements seem also to indicate a time variation of the water transparency at the ANTARES site.

The data were also analysed in order to extract the scattering length and the mean  $\cos \theta$ , where  $\theta$  is the scattering angle. Because of the 4.5 ns time resolution of the electronics, photons in the tail of the the distribution have scattered with an angle at least  $\sim 35^\circ$  ( $25^\circ$ ) for 24 m (44 m), which means that only the water properties for “large” scattering angles were measured. These are, however, the photons expected to affect the performances of a neutrino telescope, since the photons scattered at low angles are included in the bulk of direct photons. In the future, the time resolution of the test will be improved in order to be sensitive to smaller scattering angles.

The data were nicely reproduced with an absorption length in the range (55-65) m, a scattering length at large angle greater than 200 m and a correspondingly roughly isotropic scattering angle distribution. The light scattering will not limit the angular resolution of the telescope.

### 3.2. Optical background

The trigger logic and the electronics have to take into account the presence of the deep sea optical background, which affects as well the quality of the event reconstruction. This optical background consists of bioluminescent light and a constant contribution from the natural sea water radioactivity. It was measured during several sea campaigns.

The  $\beta$ -decay of  $^{40}\text{K}$  gives a low amplitude contribution to the optical background; the rate is about 20 kHz when measured with a 8" PMT with a threshold at 0.3 pe. A similar rate can be reached by a bioluminescent component with a slow time variation (typically, a time scale of few hours). Optical modules as far away as 40 m record the same variations of this component. In the top of that, bioluminescent bursts of a few ms rise-time, decaying within 1 or 2 seconds, were also detected. The counting rate can reach tens of MHz, but the phenomenon is local: only neighbouring optical modules with a separation smaller than 1.5 m see them simultaneously.

The bioluminescence rate (defined as fraction of time when an OM counts more than 200 kHz) is strongly correlated with the current speed and shows also seasonal variations. When integrated over the measured distribution of counting rates, the dead time induced on the electronics for the whole detector is less than 5%, randomly distributed over the detector due to the local character of the bioluminescence bursts.

#### 4. Detector performance

Software packages for physics and detector simulation were developed in order to estimate the detector performances and to optimize its geometry for the interesting physics channels. Effort went into creating a detector design which ensures suitable performances over a large energy range for neutrinos.

The problem is not trivial: the low energy ( $\leq 500$  GeV) and the high energy neutrino events occur in distinct detection regimes. The first are contained (in the sense that the neutrino interaction point is contained in the detector active volume), whereas the second are completely dominated by the non-contained events, when the muon is generated in a neutrino charged current interaction far from the detector volume, but it has enough energy to be detected.

In both regimes, the neutrino detection is based on the reconstruction of the associated muon track. The geometrical track is fitted using a likelihood function based on the hit PMTs time and spatial information [4]. The energy reconstruction is different for the two regimes. For the low energy, contained muons, the energy is estimated with their range. Higher energy muon tracks exceed the detector dimensions, but above few TeV, the energy loss is dominated by the catastrophic losses and linear in the muon energy. An algorithm was developed to estimate the energy using the overall amplitude of the recorded hits [5].

In all the simulations leading to the results presented in the following, the optical background coming from the  $^{40}\text{K}$  was included. Filters were developed to remove them.

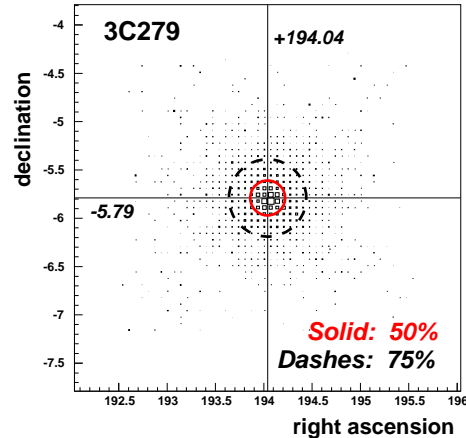


Figure 3. Simulations were made supposing the AGN 3C279 a point source of neutrinos. The events were simulated in a year time of data taking, taking into account the Earth dynamics and the absorption of the high energy neutrinos in the Earth. Half of the events selected after the reconstruction point back to a pixel of radius less than  $0.2^\circ$  around the true source.

##### 4.1. Astrophysics

In the high energy regime, the expected performances fully qualify the detector for neutrino astronomy: the angular resolution for neutrinos with a  $1/E^2$  spectrum is estimated to be  $0.2^\circ$ . Supposing a point source of neutrinos, half of the reconstructed and selected events would point back at less than  $0.2^\circ$  from the real neutrino source (Figure 3). The angular error is comparable to the angular resolution of the present high energy  $\gamma$  ray telescopes.

Figure 4 shows the effective detector area as a function of the true muon energy, for those events which (in order) trigger the detector, are reconstructed and satisfy the selection criteria. The convolution of the last one with the predicted flux of neutrinos leads to the expected rates.

The error on the muon energy (a factor of 3 for energies below 10 TeV and a factor of 2 above 10 TeV) allows the reconstruction of the energy spectra; for diffuse cosmic neutrinos a cut on the reconstructed energy is the only way to control

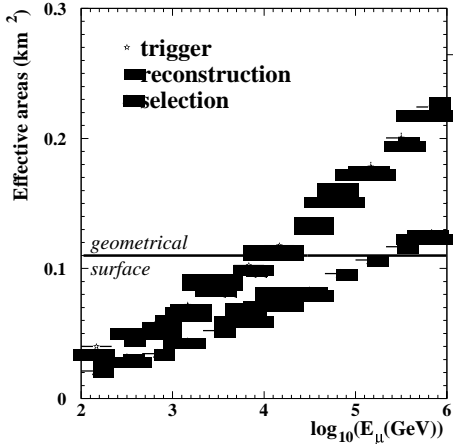


Figure 4. Effective area for triggering, reconstructed and selected events, averaged for muons coming from the lower hemisphere.

the signal contamination with atmospheric neutrinos and the estimated energy resolution ensures an efficient separation of the cosmic neutrinos [5]. A cut on the reconstructed energy at 10 TeV (100 TeV) leads to an estimate rate (events/year) for the atmospheric neutrinos of 70 (1), to be compared with 220 (65) events/year predicted in [6] for the diffuse neutrinos from AGNs, or 34 (21) events/year from blazars [7].

The search for point sources of neutrinos does not require a high energy threshold; the good angular resolution reduces the atmospheric background to a very low level, as soon as a small angular region of the sky is selected. Practically no background is expected for the GRB neutrinos, which are point-like not only in their origin, but also in time.

Even if the detection of the brightest individual sources of neutrinos could require several years of data taking, a statistically significant effect could be detected in one year in a 0.1 km<sup>2</sup> detector by adding the contributions of all the extragalactic sources. The expected number of events is between 10 and 100 (depending on the theoretical model), to be compared to a background of about 3 events [1].

## 4.2. Neutrino Oscillations

The measurement of the atmospheric neutrino flux for energies below 100 GeV allows the neutrino oscillation study for neutrino mass difference  $\Delta m^2$  between  $10^{-3}$  and  $10^{-4}$  eV<sup>2</sup>. The analysis carried out to estimate the sensitivity of the proposed experiment to the neutrino oscillation parameters  $\Delta m^2$  and  $\sin^2 2\theta$  is based on partially contained events. The number of signal events was calculated using the presently known values for the flux of atmospheric neutrinos and the expected experimental acceptance. The neutrino flight distance  $L_\nu$  is related to the neutrino zenith angle  $\theta$  by  $L_\nu = L_0 \cos \theta$ , where  $L_0$  is the diameter of the Earth (taken as a perfect sphere of diameter 12740 km). The neutrino energy is reconstructed using the muon detected range.

The histogram in figure 5 shows the distribution of the accepted events as function of  $E_\mu/(L_\mu/L_0)$ , where  $E_\mu$  is the energy and  $L_\mu$  the oscillation length corresponding to the reconstructed muon tracks, in the absence of the oscillations. The statistics corresponds to three years of data taking. The “data” points in the same figure represent the same simulated events, but in an oscillation scenario, ie weighting each event with the survival probability  $P = 1 - \sin^2 2\theta \sin^2(1.27\Delta m^2 L_\nu/E_\nu)$  (with the true neutrino values  $E_\nu$  and  $L_\nu$ ).

To explore the  $\Delta m^2$  and  $\sin^2 2\theta$  parameter space and to simulate different data-taking experiments, a large number of “three year” simulations were carried out for different points in the parameter phase-space, each one producing a distribution of “data” points like the points represented in figure 5. Each of these distributions were compared to a high statistics simulation without oscillations.

The ratio oscillations/no oscillations for the different simulations were used to find the regions in the parameter phase-space that could be excluded if no oscillations are found in the data and to estimate the accuracy with which the oscillation parameters can be extracted from the data if they are found. To remove the effect of the absolute normalization, the no-oscillations distribution is multiplied by a free parameter for each of the “three-year” simulations. Figure 6 shows the re-

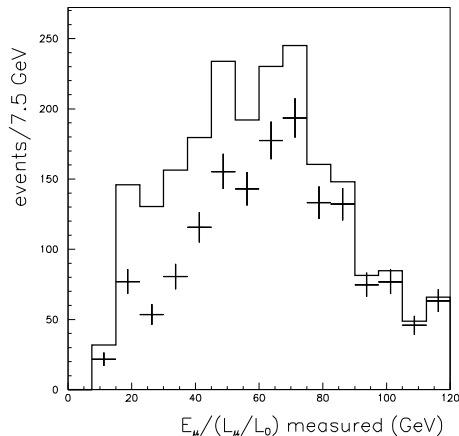


Figure 5. Simulated number of events in 3 years with no oscillations (histogram) and with oscillations (points) for  $\sin^2 2\theta = 1.0$  and  $\Delta m^2 = 0.0035 \text{ eV}^2$ .

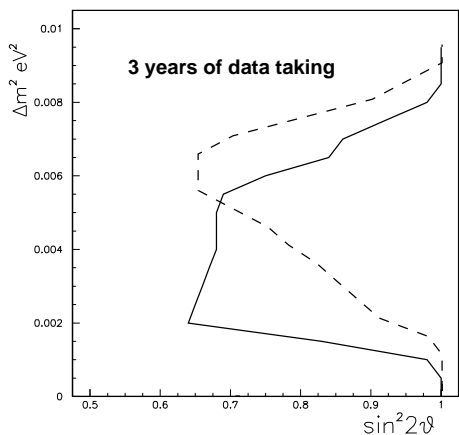


Figure 6. For three years of data taking, neutrino oscillations could be excluded at 90% CL in 80% of the simulated experiments in the region to the right of the solid curve. With the same statistics, the oscillation parameters  $\Delta m^2$ ,  $\sin^2 2\theta$  can be measured with fractional error less than 33% in more than 80% of experiments in the region to the right of the dashed curve.

gion of parameters where the neutrino oscillations could be excluded at 90% CL in 80% of the simulated experiments, as well as the region where both  $\Delta m^2$  and  $\sin^2 2\theta$  can be measured with an error less than 33% in more than 80% of the experiments. The measurement region is shifted up in  $\Delta m^2$  compared to the exclusion region because of the low-energy cut-off in the acceptance. A range of  $E/L$  values around the minimum of the survival probability is needed to find the precise position of the minimum and make an accurate determination of  $\Delta m^2$ , whereas a measurement of a number of events at the calculated position of the minimum is sufficient for exclusion.

## 5. Conclusions

Most of the technical aspects relating to the construction and operation of a deep sea neutrino telescope have been addressed within the ANTARES project.

The site evaluation program lead to the identification of a site with environmental parameters suitable for the next stage of the project: the construction of a 1000 PMTs detector, with an effective area of about  $0.1 \text{ km}^2$ . A prototype string, with 8 PMTs and connected to the shore will be deployed in the summer 99.

The scientific program includes neutrino astronomy, indirect detection of non-baryonic dark matter and search for neutrino oscillations.

## REFERENCES

1. ANTARES proposal, astro-ph/9907432.
2. Fukuda, Y. 1998, Phys. Lett. 81, 1562.
3. N. Palanque-Delabrouille, proceedings ICRC 99, HE 6.3.20.
4. P. Payre in "Simulation and Analysis Methods for Large Neutrino Telescopes", DESY-Zeuthen, Germany, July 6-9, 1998, DESY-PROC-1999-01.
5. F. Hubaut, PhD thesis, Université de la Méditerranée, Aix-Marseille II (1999).
6. L. Nellen, K. Mannheim, P.L. Biermann, Phys. Rev. D47 (1993) 5270.
7. R.J. Protheroe, ADP-AT-96-7 and astro-ph/9607165.